

Why should Models of Dwarf Galaxy Evolution care about the Initial Mass Function at low Star-formation Rates?

P. Steyrleithner^{*}, G. Hensler

Department for Astrophysics, University of Vienna, Türkenschanzstrasse 17, A-1180 Vienna, Austria

Accepted XXX. Received YYY; in original form ZZZ

ABSTRACT

When star clusters are formed at low star-formation rates (SFRs), their stellar initial mass function (IMF) can hardly be filled continuously with stars at each mass. This lack holds for massive stars and is observationally verified by the correlation between star-cluster mass and its most massive cluster star. Since galaxy evolution is strongly affected by massive stars, numerical models should account for this lack. Because a filled IMF is mostly applied even when only fractions of massive stars form, here we investigate by 3D chemo-dynamical simulations of isolated dwarf galaxies how deviations from a standard IMF in star clusters affect the evolution. We compare two different IMF recipes, a filled IMF with one truncated at a maximum mass at which a single complete star forms. Attention is given to energetic and chemical feedback by massive stars. Since their energy release is mass dependent but steeper than the negative IMF slope, the energetic feedback retains a positive mass dependence, so that a filled IMF regulates SF stronger than truncated IMFs, though only stellar number fractions exist. The higher SFR of the truncated IMF in the simulation leads to more supernovae II (SNeII), driving galactic winds. Whether this results from the model-inherent larger SFR is questioned and therefore analytically explored. This shows the expected result for Lyman continuum, but that the total SNeII energy release is equal for both IMF modes, while the power is smaller for the truncated IMF. Reasonably, the different IMFs leave fingerprints in abundance ratios of massive-to-intermediate-mass star elements.

Key words: hydrodynamics – methods: numerical – galaxies: dwarf – galaxies: evolution – galaxies: star formation – stars: luminosity function, mass function

1 INTRODUCTION

Stars are born in galaxies obeying a particular mass distribution, the so-called initial mass function (IMF). Originally defined by [Salpeter \(1955\)](#) as the number of stars $N(m)$ in a mass bin dm from local star counts, it was believed for a long time that this IMF should be universal. Individual observations and comprehensive surveys with advanced techniques over the last two decades, provide deeper insights into the IMF of star clusters, but also raise doubts on the universality of the IMF.

The IMF is one of the most important distribution function in astrophysics, because it determines the mass-to-light ratio M/L and the baryonic fraction of the dynamical mass of galaxies as well as the transformation efficiency of gas to stars due to the mass-dependent stellar feedback. It is widely believed that the majority of stars is formed in as-

sociations, e.g. [Lada & Lada \(2003\)](#). In molecular clouds each star/binary is formed from the individual denser cores (clumps) which consist of sizes and mass scales comparable with those of individual star clusters. The core-mass function (CMF) is already close to the IMF ([Lombardi et al. 2015](#)). How the CMF develops from the divergent cloud mass function and how it transforms to a universal IMF is still a field of active debate and rapid progress ([Krumholz et al. 2019](#); [André et al. 2019](#); [Pelkonen et al. 2021](#)).

As part of the IMF, massive stars have the shortest lives and release the most energy, mass, and heavy elements per stellar mass to their environment. Vice versa, the long-living, less active low-mass stars accumulate the stellar mass budget. By this, the IMF governs the evolution of galaxies and star clusters and determines the mass-to-light ratio M/L of galaxies. For stars more massive than the sun, the IMF can be approximated by a single power-law of -2.35 ([Salpeter 1955](#)). More refined analyses accounting also for the low-mass range ([Kroupa 2002](#)) have unveiled a multi-power-law

^{*} E-mail: steyrleitp21@univie.ac.at

function as more appropriate with a lower and more evenly inclining slope at mass ranges below $0.1 M_{\odot}$. Today the IMF by Kroupa (2001) with a three-part power-law is widely used and considered equal to that of Chabrier (2003).

The mass distribution of embedded star clusters $N(M_{ecl})$ can also be described by a single power-law with increasing number of low-mass clusters (see discussion in Elmegreen (2006)). In addition, there are two further correlations which are deduced from observations and are of relevance for the strategy of stellar mass distributions: i) Reasonably, the maximum young cluster mass $M_{cl,max}$ in a galaxy depends on the galactic star-formation rate (SFR) as found by Larsen (2002); Weidner & Kroupa (2005); Johnson et al. (2017) for a correlation of $M_{cl,max}$ with the SFR column density Σ_{SFR} . ii) Compiling the most massive star m_{max} of star clusters with their masses M_{cl} from the literature, Weidner et al. (2010) find a striking correlation comparable to those derived analytically by Elmegreen (2000) and modeled by Bonnell et al. (2003). However, Andrews et al. (2013, 2014); Weisz et al. (2015); Dib et al. (2017) find no evidence of a m_{max} dependence on the cluster mass. To study the existence of m_{max} Popescu & Hanson (2014) perform 25 million simulations of random stellar mass distributions and find that an uppermost mass range exists instead of a single m_{max} and also analytically derive a relation of $m_{max} \propto M_{cl}^{1/1.35}$.

Weidner & Kroupa (2006) performed Monte Carlo simulations to establish this $m_{max} - M_{cl}$ correlation observationally. They randomly take clusters from an embedded cluster mass function and fill them with stars from an IMF either with or without an upper mass limit, thereby reaching single-star or randomly sampled or sorted clusters. They come to the conclusion that an IMF populated with stars randomly and without a mass limit do not match the observations. The scatter in m_{max} with the cluster mass can thereby be understood to emerge from observational uncertainties only (Weidner et al. 2013).

As a consequence of correlation ii), a lack of massive stars has to exist in low-mass clusters, called top-light IMF, and equal to a dominance of low-mass stars, called bottom-heavy IMF, if one focusses on the low-mass part. This fact is observationally manifested through various indicators, e.g. by stellar population analysis of galaxies with different masses, low-surface brightness galaxies (LSBs) (Lee et al. 2004), early-type galaxies (ETGs) (Conroy & van Dokkum 2012), and massive cluster galaxies (Loubser et al. 2020), or by the spectral signatures as there are $H\alpha$ vs. UV (Calzetti et al. 2010; Lee et al. 2009), and furthermore, by chemical abundance analyses (Tsujiimoto 2011; McWilliam et al. 2013). Moreover, ETG studies also reveal possible correlations of the IMF slope with velocity dispersion (Ferreras et al. 2013; Martín-Navarro et al. 2015) and metallicity (Martín-Navarro et al. 2015) in the sense of a steeper IMF slope with larger velocity dispersion and metallicity, respectively.

Dwarf galaxies (DGs) are the most numerous type of galaxies in the universe. They have low surface brightness, low gravitational potential wells and relatively low SFRs. This latter property questions whether the IMF can be filled up to the most massive stars or is truncated at a low but massive limit according to ii). In fact, Lee et al. (2004) find a much steeper power-law exponent than Salpeter or Kroupa and favored a bottom-heavy IMF. Due to their low gravita-

tional potential wells, DGs react more vigorously to external and internal processes such as feedback by massive stars and are therefore ideal objects to study galaxy evolution.

Lee et al. (2009) compare SFRs derived from the $H\alpha$ flux, a tracer for the most massive O-stars ($m_* \geq 17 M_{\odot}$), with that from the FUV flux, a tracer for O-to-early-B stars ($m_* \geq 3 M_{\odot}$) of a sample of ~ 300 star-forming galaxies within 11 Mpc distance from the Milky Way. They find that $H\alpha$ -to-FUV flux ratios are up to one order of magnitude lower than expected for SFRs below $10^{-2} M_{\odot} \text{ yr}^{-1}$. They conclude that an IMF which is deficient of massive stars in DGs and LSBs is consistent with their data because the $H\alpha$ luminosity flattens at very low SFRs (Pflamm-Altenburg et al. 2007). This $H\alpha$ -to-FUV flux divergence at low SFR is also documented by Meurer et al. (2009) as is the decreasing ratio of stellar ionizing to non-ionizing flux with smaller galaxy luminosity and mass, as well as a lower SFR (Meurer et al. 2009; Boselli et al. 2009). Calzetti et al. (2010) find that a tendency towards a decreasing $H\alpha$ luminosity-to-cluster mass M_{cl} exists, but not as strong as expected from ii). Although by a simple understanding, the $H\alpha$ -to-UV discrepancy of the derived SFRs can be explained by the lack of massive stars caused by a truncated and/or a steeper IMF, additional explanations are elaborated. To solve this discrepancy, Fumagalli et al. (2011) study the stochastic sampling for a universal IMF at low SFRs of DGs and vary the fractions of cluster-born vs. field stars. Another strategy is proposed by Weisz et al. (2012), applying short-term (+10 Myr) SFR episodes timely separated by one to a few hundred Myr, which matches the observations much better than a variable IMF alone. A further successful exploration is performed by Eldridge (2012) for a purely stochastic sampling of the IMF with the inclusion of binary-star formation. Interestingly, Roychowdhury et al. (2009) find from UV data of extremely faint DGs taken with the GALEX satellite, no threshold of the SFR with the gas column density Σ_{HI} as it is suggested by Kennicutt (1998). Σ_{SFR} reaches down to $10^{-6} M_{\odot} \text{ yr}^{-1} \text{ kpc}^{-2}$ and is only limited by the GALEX sensitivity. These results support the $m_{max} - M_{cl}$, $M_{cl,max} - \text{SFR}$ correlations explained by the hierarchical approach of SF (Elmegreen et al. 2014).

In addition to that, Weidner et al. (2013) argue that fainter galaxies have steeper IMF slopes than brighter (more massive) ones. This agrees with observational hints that massive galaxies with large SFRs are sites of a top-heavy IMF (Taylor et al. 2011; Kroupa et al. 2013; Nagashima et al. 2005). Baugh et al. (2005) also find from semi-analytical models using submillimeter observations that the observed counts from early submillimeter galaxies (SMG) samples can only be matched by adopting a very top-heavy IMF. Nagashima et al. (2005) stated that only extreme top-heavy IMFs can explain the properties of elliptical galaxies and Weidner et al. (2013) suggest that "an early strong star-bursting stage with a top-heavy IMF" must have existed for ETGs, followed by a second epoch with (probably) a bottom-heavy IMF. This argument for a coexistence of both possibilities is also pointed out in the review of Smith (2020).

If the SF is concentrated to a single region, two extreme cases of SF are observed. Star clusters with very low SFRs can e.g. be formed in very dilute gas environments like e.g. in tidal tails of interacting galaxies, e.g. Lee-Waddell et al. (2016, 2018), and in ram-pressure stripped gas clouds of cluster galaxies, e.g. Boselli et al. (2018). A rough estimate al-

ready prohibits an IMF from being completely populated (Ploeckinger et al. 2014). The other extreme is so-called super star clusters produced in starburst DGs, which seem to violate the $M_{cl,max}$ -SFR relation. Moreover, the deterministic vs. stochastic massive star formation is under debate observationally (Andrews et al. 2014) and theoretically (see e.g. reviews by Kroupa (2014) and Krumholz (2014)). That the stochastic population of e.g. 100 clusters of $1000M_{\odot}$ must produce the same numbers and masses of massive stars as a single 10^5M_{\odot} cluster and represent a fully sampled IMF is in contrast to the $m_{max} - M_{cl}$ and $M_{cl,max} - \text{SFR}$ correlations. These require a smaller total number of massive stars in numerous clusters than the single cluster, which must lead to differences in the stellar feedback, in terms of energetic as well as chemical yields.

On the other hand, the validity of $H\alpha$ as SFR equivalent must be also questioned, because stellar feedback can cause the $H\alpha$ flux to both underestimate (Andrews et al. 2013) and overestimate (Melekh et al. 2015) the SFR. Andrews et al. (2014) demonstrate strikingly that a limitation of the uppermost stellar mass leads to a reduced $H\alpha$ emission from a star cluster as a result of lacking Lyman continuum photons. In DGs superbubbles from accumulated type II supernovae (SNeII) can open holes in the interstellar medium (ISM) around star clusters and allow the escape of Lyman continuum (Ly_c) photons. This leakage has to depend on the shape of the DG disk (Recchi & Hensler 2013). Analysing these models Melekh et al. (2015) find an escape fraction of about 40%, but also that additional Ly_c photons from cooling hot superbubbles raise the $H\alpha$ emission by a factor of about 1.5.

Numerous numerical simulations of DGs have been performed over the last two decades studying the influence of SF on the DG evolution, but also the various internal/external processes that determine the formation and evolution of isolated DGs. Valcke et al. (2008) identify the role of angular momentum as a second parameter (Schroyen et al. 2011), and according to this, the minimum disk column density for SF (Vorobyov et al. 2012) and the interplay between mass and geometry as important effects of galactic wind and the distribution of heavy elements (Recchi & Hensler 2013). Further focus was set to the formation and evolution of particular morphological DG types with regard to SF and chemical abundances such as e.g. tidal-tail DGs (TDGs) (Ploeckinger et al. 2014, 2015; Baumschlager et al. 2018), ram-pressure stripped DGs (Steyrleithner et al. 2020) and also of dwarf ellipticals (dEs) (Hensler et al. 2004), applying advanced chemo-dynamical multi-phase numerical codes. These simulations include self-consistently radiative gas cooling, SF stellar feedback by radiation, winds, type Ia and II SNe. Those yield temporarily very low SFRs. Since it is computationally too demanding to resolve single stars in a galactic simulation, formed star clusters have to be treated as single stellar populations (SSPs) containing stars of all masses within an IMF range.

To determine the correct feedback from stars, depending on their mass and lifetime, the IMF must be implemented properly. Since the IMF is thought to be invariant through large ranges of conditions (Kroupa 2001), this assumption is used to describe individual clusters numerically. For simplicity, most simulations take the universal but fully populated IMF into account, whereas, especially for low-mass DGs with

their low SFRs, the formed star-cluster mass is too small to fill the IMF. Filling means that each mass bin, independent of the binning width, up to m_{max} contains at least one star of that mass. Therefore in this case, two options are plausible to populate the IMF: either it can be truncated at an uppermost mass m_{max} that holds at least one integer star, or the IMF is filled stochastically. Elmegreen (2009) shows that even the latter mode mostly fills the IMF of low-mass star clusters up to a characteristic upper mass that stays, however, below the possible maximum. How a filled vs. truncated IMF affects the evolution of TDGs is already demonstrated by us (Ploeckinger et al. 2014). For a truncated IMF, these models experience a stronger SF and thus form more stars as a consequence of lower self-regulating energy. The energetics of both IMF modes are also compared on the basis of stellar lifetime, i.e. as feedback power, but without a quantitative analysis.

Bekki (2013) performs 3D hydrodynamical simulations of galaxy evolution with a universal and a non-universal IMF, respectively, and finds that the SFRs in the non-universal IMF model are lower than for the universal IMF. He also show that the IMF slopes can vary in different galaxies, but also in different local SF regions within the same galaxy. Having spotted this problem, Applebaum et al. (2020) model DGs, applying a cosmological Smoothed-particle Hydrodynamics (SPH) code with feedback from massive stars and gas physics, and implement a self-consistent stochastically populated IMF. In comparison, they find that a continuous IMF yields a higher stellar mass, which is caused by the lower feedback of discrete supernova explosions due to overcooling and which result in a higher SFR. Unexpectedly, they do not find significant variations of chemical abundances. IMF variations at the massive-star range must become discernible in particular ratios of elements enriched by intermediate-mass stars (IMS) vs. massive stars. Most obviously, the abundance ratio of C produced by IMS to O released by massive stars should be sensitive to an uppermost mass cut-off or a top-down of the IMF. Tsujimoto & Bekki (2011) analyze C/O ratios of Damped Lyman Alpha systems (DLAs) and conclude from the observed high values that these indicate a nucleosynthesis production dominated by stars less massive than $20 - 25M_{\odot}$.

Since the energetic feedback of massive stars by both, SNeII, stellar radiation and winds, plays a substantial role in DG evolution, the mass range of massive stars is a sensitive ingredient for galactic energetics and chemistry. The feedback of massive stars becomes even more pronounced in the shallower gravitational potential of DGs which facilitates galactic winds.

Equally sensitive impacts of different stellar masses come from their chemical yields, because those are clearly dependent on the stellar progenitor mass, so that abundance ratios of characteristic elements attributable to intermediate vs. massive stars bear the key to deviations of the IMF.

This paper aims at quantifying the effect of the numerical simplification, assuming a filled IMF while reaching only low SFRs, so that only stellar mass fractions are theoretically populating the massive-star range. Moreover, we aim at sensitizing galaxy modelers to the evolutionary impact of lacking massive stars in low-mass star clusters. In addition, we wish to understand and quantify the (former) findings in

TDG models (Ploeckinger et al. 2014) as to why the stellar feedback to the local star-formation process is stronger for a truncated IMF and whether its SNeII energy release is only caused by the larger SFR or more by the integer numbers of SNeII explosions. The paper is therefore structured as followed: Sec. 2 gives an overview of the code used, the initial conditions and the implemented processes such as SF, cooling and feedback. Sec. 3 describes the results which are discussed in sec. 4, with the focus on an analytical understanding of the numerical results. Finally, sec. 5 draws conclusions from our models.

2 SIMULATIONS

2.1 The Code

In this work we use our simulation code cdFLASH, which is an extension of the FLASH code version 3.3 (Fryxell et al. 2000) by several chemo-dynamical ingredients such as, amongst others (see the following subsections!), gas-dependent star-formation recipe, stellar-mass dependent release and trace of chemical element abundances, and their effect on gas cooling. These code extensions are successfully applied to various astrodynamical aspects like TDG evolution (Ploeckinger et al. 2014, 2015; Baumschlager et al. 2018) and ram-pressure stripping (Steyrleithner et al. 2020). A repetition of the FLASH code ingredients and specifications is avoided here and can be inspected in (Steyrleithner et al. 2020).

2.2 Initial Conditions

Our models are aimed at starting with a purely gaseous disk, embedded in an existing stationary DM halo and are the same as in Steyrleithner et al. (2020) (see fig.1). Since the energetics of SF and gas dynamics are determined by the gas structure itself and the total gravitational potential, we include for simplicity an old existing stellar population into the DM mass. For a clear determination of the SF effects by the massive stars of the IMF modes, the mass and energy contribution by the old population is assumed to be terminated. Although we are aware that this is not truly realistic cosmological scenario, having also neglecting a temporal mass growth of such low-mass systems, for our purposes it is sufficient to focus on the newly formed stars and their effects. The models are executed in a 3D box of ± 12 kpc grid size and a six-level mesh refinement so that the highest resolution reaches 50 pc, i.e. less than 1/3 of the disk scaleheight. This spatial resolution is also justified by the observed scales of star-forming molecular clouds and the range of separations of young star clusters.

For the initial conditions of a stable disk the code described by Vorobyov et al. (2012) is used to calculate an equilibrium configuration of a rotating gas disk, where the steady-state momentum equation for the gas component in a gravitational potential due to gas and DM is solved, as described in detail in Steyrleithner et al. (2020, see sec. 2.2). Although the initial mass setup is analytically an equilibrium state, we relax the model numerically for another 230 Myr before the physical processes as e.g. SF, cooling, etc. are switched on.

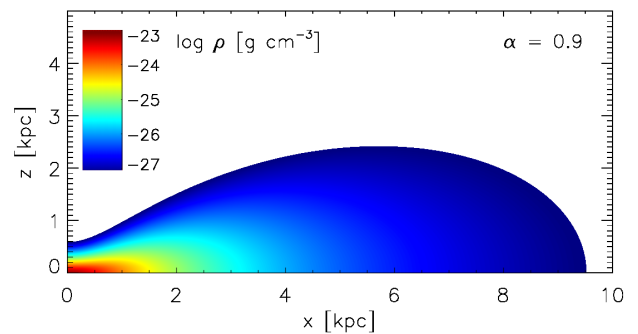


Figure 1. Initial gas density in an edge-on cut through the galaxy center. The colour bar gives the logarithmic scale of the volume densities.

Most simulations of isolated galaxies neglect self-gravity in building the initial configuration, so our approach is an improvement compared to commonly used methods (Vorobyov et al. 2012, 2015). For the DM halo a spherical isothermal density distribution is assumed.

We simulate two DGs with identical initial conditions: In one simulation all mass bins of the IMF are filled, according to the Kroupa IMF, until an upper mass (that does not depend on the cluster mass) of $m_{max} = 120 M_{\odot}$, allowing the formation of fractions of massive stars. In the other simulation the IMF is truncated at an uppermost mass, at which the next bin would contain less than one full star.

For a given halo mass of $M_{DM} = 10^{10} M_{\odot}$ and a spin parameter of $\alpha = 0.9$ the resulting gas mass is $M_g = 1.4 \times 10^8 M_{\odot}$ with a maximum rotation velocity of $v_{rot} = 30 \text{ km s}^{-1}$. The radius R_{gal} of the DG is defined to be the radial distance at which the gas density falls below $10^{-27} \text{ g cm}^{-3}$ and amounts to $R_{gal} = 9.5 \text{ kpc}$. For regions outside of R_{gal} , the gas density is set to $10^{-30} \text{ g cm}^{-3}$ and the temperature to $T = 10^6 \text{ K}$ to be in pressure equilibrium with the galaxy. The DM mass within R_{gal} amounts to $M_{DM,in} = 8.4 \times 10^8 M_{\odot}$.

The choice of such a low-mass DG is also made in order to get low SFR and stellar cluster masses that will not fill the stellar initial mass function. With higher gas masses the SFR increases, which will result in more massive cluster masses that fill the IMF. The initial metallicity in our simulations is based on $Z = 0.32 Z_{\odot}$.

2.3 Cooling

For the radiative gas cooling, two cooling functions are used and described in detail in (Steyrleithner et al. 2020, see sec. 3.1). Since the stellar mass loss is also specified for the chemical elements, the cooling function above 10^4 K by Boehringer & Hensler (1989) assumes collisional ionization equilibrium and depends on the ten most abundant elements (H, He, C, N, O, Ne, Mg, Si, S, Fe) and transits smoothly to bremsstrahlung above several 10^7 K . Below 10^4 K , a combination of the cooling functions by Dalgarno & McCray (1972) & Schure et al. (2009) is applied, for which the elements C, N, O, Si, S, Ne and Fe and the electron collisions for these elements are taken into account, and which are given by a series of equations (eq. 4 - 12, Schure et al. 2009).

The total cooling function is the sum of the cooling of these elements.

2.4 Star Formation

For the SF the fully analytically derived SFR formula of self-regulation by Koeppen et al. (1995) is applied:

$$\psi(\rho, T) = C_n \rho^n f(T) \quad (1)$$

with a power-law dependence on the gas density ρ and a temperature T efficiency function with an efficiency factor C_n . $f(T)$ is an exponential function of

$$f(T) = e^{-T/T_s} \quad (2)$$

that accounts for the maximum star formation at low temperatures, but a smooth transition to almost 0 close to ionized gas. T_s is therefore set to 1000K. For the optimal value Koeppen et al. (1995) found $n = 2$ in agreement with the prescription by Larson (1988). C_2 then amounts to $2.575 \times 10^8 \text{ cm}^3 \text{ g}^{-1} \text{ s}^{-1}$ so that ψ of eq. 1 gets the meaning of a SFR density and is called "stellar birth function" (SBF). Since a fraction of the gas is already ionized by the stellar radiation of massive stars around star particles, the total amount of gas available for star formation has to be reduced by these HII regions and heated according to stellar feedback (see subsec. 2.7.3) so that the SFR in a closed cell would decline from timestep to timestep.

Each SF event should produce a stellar particle that represents a single stellar population in simulations. Since eq. 1 allows SF even at very low rates leading to insignificantly low-mass star clusters and artificially numerous stellar particles, a stellar particle is generated only when a certain threshold of SFR density

$$\psi_{thres} = \frac{\theta_{sf} M_{cl,min}}{\tau_{cl} V_{GMC}} \quad (3)$$

is exceeded. ψ_{thres} combines θ_{sf} as a dimensionless factor and is set to 100, a minimum cluster mass set to $M_{cl,min} = 100 M_\odot$ and the cluster-formation timescale τ_{cl} of 1 Myr as used in Ploekinger et al. (2015); Baumschlager et al. (2018); Steyrleithner et al. (2020) to be a reasonable timescale for the pre-main sequence formation of massive stars. V_{GMC} as the volume of a giant molecular cloud (GMC) and the density are derived from the Larson (1988) relations. Taking e.g. a radius $R_{GMC} = 200 \text{ pc}$ into account with a resulting volume of $V_{GMC} = 3.35 \times 10^7 \text{ pc}^3$ ψ_{thres} results to $2.984 \times 10^{-4} M_\odot \text{ Myr}^{-1} \text{ pc}^{-3}$. While for a smaller V_{GMC} ψ_{thres} and, by this, also the SFR decreases, the minimum spatial resolution of 50 pc (subsec. 2.2) facilitates cluster formation within the same GMC but separated by neighbouring grid cell and according with observed separations of young star clusters.

For the formation time of a star cluster we make the following Ansatz: The free-fall time for a dense core is of the order of $10^4 - 10^5 \text{ yr}$. As we know, this would lead to a SFR in our Milky Way molecular clouds of $\sim 100 M_\odot \text{ yr}^{-1}$. This is almost 2 orders of magnitude larger than the actual SFR, so that the formation time for stars and thus also for a cluster should be of the order of 1 Myr. As an order of magnitude this also accounts for the gas disruption by SNeII of the Myr-living massive stars.

The short cluster-formation time τ_{cl} also ensures a quick

start of the stellar feedback, which is important for a self-regulated SF. If the τ_{cl} is larger than 1 Myr, then the stellar particles still accrete mass from surrounding cells, which also fulfils the SF criteria, although massive stars should have already started to act by their feedback. If the SF criteria are fulfilled, stars can form, but subsequent SF will be affected by stellar feedback from previous generations.

Our SF algorithm can be explained as follows: If the SF criteria $\psi > \psi_{thres}$ is fulfilled, the newly formed stellar particle will have the mass

$$dm = \psi \cdot dt \cdot V_{cell}, \quad (4)$$

where dt is the numerical time step and V_{cell} the volume of the computational cell in which the SF occurs. During the cluster-formation time of τ_{cl} the stellar particle acts as a sink particle. Each timestep the particle will accumulate mass according to eq. 4, if the SF criteria is fulfilled in the corresponding cell. When the particle age exceeds the cluster-formation time τ_{cl} , the sink particle will be closed for further mass accretion and start its life as a SSP with stellar feedback (see subsec. 2.7). The sum of the accumulated mass of this particle is then the cluster mass M_{cl} .

2.5 Uncertainties of Parameter Choices

As in all numerical treatments of subgrid physics of star-formation parametrization a reasonable discussion of the arbitrarily chosen parameters with respect to the effects on the results should be presented. Although the here applied evolutionary method was seriously tested and applied to various objectives from TDGs (Ploekinger et al. 2014, 2015; Baumschlager et al. 2018), to ram-pressure stripped DGs (Steyrleithner et al. 2020), all applying the FLASH code, and also to dEs (Hensler et al. 2004), we wish to roughly discuss two parameter choices for our star formation recipe: The influence of the cluster formation time τ_{cl} in eq. 3 and the volume of a computational cell V_{cell} in eq. 4.

Since stars are formed per numerical timestep (of the order of 10^4 yr), the star cluster mass accumulates these temporal stellar mass fractions until a stellar particle is born after τ_{cl} representing a stellar cluster. Because these stellar mass fractions are continuously subtracted from the gas mass in each timestep, the gas mass M_g decreases and by this reasonably also the SFR until τ_{cl} . Due to stellar feedback (subsec. 2.7) the temperature T in eq. 2 even increases and enhances a decreasing SFR. If the SFR = $dM_s/dt = -dM_g/dt$ is proportional to the gas mass, $M_g(t)$ declines by e^{-t} , i.e. that most of a star-cluster mass is formed rapidly and after τ_{cl} M_g is reduced by $e^{-\tau_{cl}}$ so that a variance by a factor of e.g. two to both sides does not change the cluster mass significantly. In fact, the value of τ_{cl} is convincingly derived as explained above. Due to the square-dependence of the SFR in eq. 1 on the gas density, M_g declines even steeper as $1/t$ (for constant T).

With respect to the here presented comparison of both IMF modes it must be emphasized that absolute values of one IMF mode play a secondary role only as long as the parametrization is the same.

Furthermore, due to dynamical effects M_g in a grid cell will change during τ_{cl} but not be replenished of the same amount by gas inflow as it is reduced by star formation. Even more, the stellar feedback increases the gas pressure, acting against

inflow. After τ_{cl} a new generation of cluster formation can start.

Another important measure is the grid size, which lowers or rises the cell volume V_{cell} by a factor of eight for changes of the simulation resolution by a factor of two. As an extreme, one can ask how much a division of the whole galaxy into a few (1-4) grid cells would effect. Would it lead to a reasonable result, when all the star-forming regions (in the case of larger grid cells) are connected to a single super cluster? From observations star-forming molecular clouds are extended to scales from < 10 to ~ 30 pc (Faesi et al. 2019, e.g. in NGC 300) and young star clusters are separated by $30+$ pc (Grasha et al. 2019, e.g. in M51). This means that a grid resolution of 50 pc sounds reasonable for star-cluster formation. While smaller grid cells could eventually lead to complications if HII regions get larger, doubling the scale would in reality hardly comprise a single star-forming molecular cloud so that > 1 star clusters should form which would be artificially combined to one in the models.

2.6 The Initial Mass Function

Although the IMF implementation has already been basically described in Steyrleithner et al. (2020), we repeat the details here in order to explain our model strategy. Once a SSP is formed, it will immediately produce feedback in the form of stellar radiation and SNeII, depending on the mass of the SSP. The IMF is a function that describes the probability for a star of mass m to be born in the interval $[m, m + dm]$ and, by this, describes the number of newly-formed stars in each mass bin. It can be expressed by a power-law

$$\xi(m) = km^{-\alpha} \quad (5)$$

where k is a normalisation constant and $\alpha = 2.35$ (Salpeter 1955) for a single power-law or for a multi-section power-law (Kroupa 2001):

$$\alpha = \begin{cases} 0.3 & \dots & 0.01 \leq m/M_{\odot} < 0.08 \\ 1.3 & \dots & 0.08 \leq m/M_{\odot} < 0.5 \\ 2.3 & \dots & 0.5 \leq m/M_{\odot} < 100 \end{cases} \quad (6)$$

The total number of stars N_{tot} and the mass of the cluster M_{cl} can be calculated by

$$N_{tot} = k \int_{m_{min}}^{m_{max}} \xi(m) dm \quad (7)$$

$$M_{cl} = \tilde{k} \int_{m_{min}}^{m_{max}} m \xi(m) dm. \quad (8)$$

Since the IMF is a probability function, the total probability of N_{tot} is unity and determines k whereas \tilde{k} is determined by the total stellar mass. For all simulations in this work, we divide the IMF into 64 equal logarithmic mass bins and apply the standard multi-section IMF by Kroupa (2001) for $\xi(m)$ in eq. 7 and 8 above.

The total number of stars N_{tot} and mass M_{cl} of a cluster

are then given by

$$N_{tot} = k_1 \int_{m_{min}}^{0.5M_{\odot}} m^{-1.3} dm + k_2 \int_{0.5M_{\odot}}^{m_{max}} m^{-2.3} dm \quad (9)$$

$$M_{cl} = k_3 \int_{m_{min}}^{0.5M_{\odot}} m^{-0.3} dm + k_4 \int_{0.5M_{\odot}}^{m_{max}} m^{-1.3} dm, \quad (10)$$

where k_1, k_2 and k_3, k_4 are normalisation constants evaluated via the cluster mass and must fulfil the condition

$$k_1 \frac{(0.5M_{\odot})^{-0.3}}{0.3} = k_2 \frac{(0.5M_{\odot})^{-1.3}}{1.3} \quad (11)$$

and

$$k_3 \frac{(0.5M_{\odot})^{0.7}}{0.7} = k_4 \frac{(0.5M_{\odot})^{-0.3}}{0.3}. \quad (12)$$

Therefore, $k_1 = \frac{6}{13} k_2$ and $k_3 = \frac{14}{3} k_4$.

In order to fill all mass bins according to the IMF from a minimum up to a maximum mass - in these simulations from $m_{min} = 0.1M_{\odot}$ to $m_{max} = 120M_{\odot}$ - a minimum star-cluster mass of about $M_{cl} = 10^4 M_{\odot}$ is necessary (see sect. 4 and Ploekinger et al. (2014)). If one assumes a star-formation timescale of 1 Myr, cluster masses of less than $10^4 M_{\odot}$ suffice for a SFR of $\leq 10^{-2} M_{\odot} \text{yr}^{-1}$ at which the SFRs derived from *Ha* and UV start to diverge (Lee et al. 2009). This leads numerically to fractions of massive stars that cannot happen in nature.

Since one can speculate that an under-populated but full-range IMF leads to energetic and chemical consequences, this paper aims at exploring how low SFRs affect the IMF and, by this, the stellar feedback by energy and chemical abundances. Plausibly, there are two possibilities to form stars at low SFRs. Firstly, to build up the star cluster from the low-mass proto-stellar cores to more massive stars, but to stop when the last complete star is formed and the remaining gas reservoir is incapable of allowing the formation of a single more massive star. Secondly, SF is assumed to happen stochastically according to the IMF probability (Krumholz 2014). Modelling allows an additional third and, for simplicity, most used approach, namely, to fill the IMF irrespectively of the need for integer numbers of stars in each bin, until the uppermost maximum mass limit m_{max} . For SFR of $\geq 10^{-2} M_{\odot} \text{yr}^{-1}$, the incompleteness of the IMF should not occur on average, but is crucial below this value.

In this paper we intend to compare an incompletely filled IMF with that of a truncation. Incompleteness means that the massive bins can be populated with fractions of stars only while the truncation of the IMF can be realized by

$$N_{m_{max}} = 1 = k_2 \int_{m_{max}}^{m_{max} + \Delta m} m^{-2.3} dm, \quad (13)$$

where Δm means the uppermost mass bin filled with the very last single star. It should be emphasized, that in both of our realizations, the IMF is not stochastically sampled as e.g. in Applebaum et al. (2020); Smith (2021); Jeffreson et al. (2021); Gatto et al. (2017) among others. The sensitivity of the choice of Δm will be discussed in subsec. 4.2.

The differences between the filled and truncated IMF, can be analytically and numerically quantified, respectively.

For the truncated IMF, the uppermost stellar mass m_{max} is a function of the cluster mass M_{cl} and can be evaluated by

$$M_{cl} = k_3 \int_{0.1 M_{\odot}}^{0.5 M_{\odot}} m^{-0.3} dm + k_4 \int_{0.5 M_{\odot}}^{m_{max}} m^{-1.3} dm. \quad (14)$$

These eq.s 13 and 14 are solved analytically, and to now obtain m_{max} for a certain M_{cl} , a root finding method (e.g. the bisection method) is used in the numerical code.

2.7 Stellar Feedback

In our simulations we consider feedback from different sources, as there are stellar radiation and winds, SNe type Ia and II, and AGB stars. Because the latter terminate the stellar lives much later than massive stars, the mass-dependent lifetimes of stars are also a relevant ingredient. The lifetime of stars as a function of mass derived by (Recchi et al. 2009) is applied (see Steyrleithner et al. (2020)). Although the treatment of stellar feedback is already documented in Ploeckinger et al. (2014) and Steyrleithner et al. (2020), we stress its formulation here again because the understanding of the different outcomes for filled and truncated IMFs can be more obviously understood by the inspection of the formulae.

2.7.1 Stellar Radiation

To complete the self-regulation of SF by stellar feedback, stellar radiation has to be taken into account. Massive stars with a mass above $8 M_{\odot}$ emit Lyman continuum photons with a flux S_* that increases with mass and which completely ionizes the ISM within the Strömgren sphere of radius R_S , resulting in an HII region. In this hot environment, SF cannot happen, so it is self-regulated. The Strömgren sphere can be derived as the equilibrium of ionisation by Lyman continuum radiation and the recombination rate of surrounding hydrogen

$$R_S = \left(\frac{3 S_*}{4 \pi n_H^2 \beta_2} \right)^{1/3}, \quad (15)$$

where S_* is the ionising photon flux, n_H the hydrogen number density, and β_2 its recombination coefficient. The ionising photon flux by Lyman continuum radiation can be approximated by (Ploeckinger et al. 2015)

$$S_*(m) = 3.6 \times 10^{42} \left(\frac{\bar{m}}{M_{\odot}} \right)^4, \quad (16)$$

where \bar{m} is the average mass within an IMF mass bin. Depending on the resolution, the Strömgren radius can be smaller than a typical grid cell. Therefore a better sub-grid description is needed, where the mass of the HII region is calculated. The wind and radiative driven feedback (energy transfer efficiency) is determined by numerical simulations to be of the order of less than 1% only (Freyer et al. 2003, 2006; Hensler 2007). The models in these papers (e.g. for $60 M_{\odot}$) show that the bubble expands to a radius of 12.5 pc already after 10^4 yr but with declining speed and thereafter suffers shell disruption by instabilities. The temperature within the Strömgren sphere is set to 2×10^4 K so that the average temperature within a grid cell is then

the mass-weighted average between the Strömgren sphere temperature and the actual temperature of the cell.

Importantly, for the comparison of filled vs. truncated IMF the total Lyman continuum flux reads

$$Ly_c \propto \int_8^{m_{max}} S_*(m) \xi(m) dm, \quad (17)$$

so that the total radiative Lyman continuum energy of a single stellar population has to be multiplied by the stellar lifetime τ_* and amounts to

$$E_{Lyc} \propto \int_8^{m_{max}} S_* \tau_*(m) \xi(m) dm. \quad (18)$$

2.7.2 Stellar Winds

Massive stars also heat the star-forming sites by their winds. The metal-dependent mass-loss rate by winds of OB stars on the main sequence is approximated (Hensler 1987; Theis et al. 1992) by

$$\dot{m}_w = 10^{-15} \left(\frac{Z}{Z_{\odot}} \right)^{1/2} \left(\frac{L}{L_{\odot}} \right)^{1.6} M_{\odot} \text{yr}^{-1}, \quad (19)$$

where Z is the stellar metallicity and the luminosity L is calculated from the mass-luminosity relation (Maeder 1996, table 1). Within a numerical timestep Δt , therefore, a stellar mass

$$m_{w,\Delta} = \dot{m}_w \cdot \Delta t \quad (20)$$

is released by winds as long as the time since the formation of the SSP is shorter than the stellar lifetime $\tau_*(m)$. To obtain the total wind mass loss of a specific mass bin, for which a mean lifetime $\bar{\tau}_*$ of all stars in that bin and the assumption of a constant wind rate \dot{m}_w over the lifetime can be applied (but see e.g. Freyer et al. (2003)), one can calculate

$$M_{w,bin} = \dot{m}_w \cdot \bar{\tau}_* \cdot N_{*,bin}. \quad (21)$$

Hence, all the $N_{*,bin}$ stars in a specific mass bin with the average bin mass \bar{m} lose a wind mass fraction of the bin

$$f_{m,w} = \frac{M_{w,bin}}{\bar{m} \cdot N_{*,bin}}. \quad (22)$$

For the wind power \dot{E} exerted to the ISM, the final wind velocity for a star within an IMF mass bin of average mass \bar{m} is then given by

$$v_{\infty} = 3 \times 10^3 \left(\frac{\bar{m}}{M_{\odot}} \right)^{0.15} \left(\frac{Z}{Z_{\odot}} \right)^{0.08} \text{ km s}^{-1}. \quad (23)$$

As for eq. 19, this dependence is derived by Hensler (1987) from the massive-star atmosphere and wind models by Kudritzki et al. (1987). The heating of the ISM by the OB stellar winds results from their kinetic power and can be expressed for each single star as

$$\dot{E}_{kin} = \frac{1}{2} \dot{m}_w v_{\infty}^2. \quad (24)$$

Practically, the total wind energy of N_* stars of all mass bins populated with stars up to m_{max} during a numerical timestep Δt is accumulated by

$$E_{w,\Delta t} = \int_8^{m_{max}} \frac{dE_w(m)}{dt} N_*(m) dm \cdot \Delta t \quad (25)$$

While stellar radiative heating is included for the formation of HII regions around massive stars - not spatially resolved, but analytically implied as subgrid physics within the cells - the energy release by radiation + wind to the surrounding ISM within a cell can be calculated according to eq. 18 and 25, but reduced by an energy transfer efficiency ϵ_w of 5%. This value is arbitrarily assumed although Hensler (2007) derived smaller values from their models (Freyer et al. 2003, 2006, Danica Kroeger, private comm. 2006).

2.7.3 Type II Supernovae

Stars with masses larger than $m_* = 8M_\odot$ end their lives as core-collapse SNeII. The feedback taken into account is purely thermal, but the SN remnants expand due to their overpressure. For each SNII explosion an ejected energy of 10^{51} erg is applied, but reduced by an efficiency of 5%, i.e. 5×10^{49} erg per SNII is transferred into the ISM. This value is arbitrarily chosen and in the realistic range of 10% from single 1D explosions models (Thornton et al. 1998), 2% derived from superbubble-to-galactic winds in simulations (Recchi & Hensler 2013) and 1–3% from recent models of supernova-driven ISM turbulence (Chamandy & Shukurov 2020). When both gas phases are allowed to mix, the cooling timescale for the mean temperature at the total gas density is too short to provide any energetic effect on the environmental ISM. To avoid this well-known overcooling problem, we use the recipe applied by Ploeckinger et al. (2014).

The SNII rate for a SSP can be easily expressed as an analytical function of the total stellar cluster mass according to the IMF and the stellar lifetimes. In computational applications of a SSP, the number of SNeII from a mass bin is given by the number of massive stars in that bin whose lifetime $\bar{\tau}_*$ is reached by the cluster age. The mass of SNeII in a mass bin with mean mass \bar{m} then depends on the mass fraction remaining from the wind loss, and is reduced by the remnant mass, which ranges between 1.3 and $2.1M_\odot$ for initially massive progenitors:

$$f_{m,rem} = \frac{m_{rem}}{\bar{m}}, \quad (26)$$

$$f_{m,SNeII} = 1 - f_{m,rem} - f_{m,w}. \quad (27)$$

From this the total SNII mass loss of a bin results from $f_{m,SNeII}$ multiplied by $N_{*,bin}$ and \bar{m} .

2.7.4 Asymptotic Giant Branch Stars

Stars with masses below $m_* = 8M_\odot$ return mass to the ISM during the asymptotic giant branch (AGB) phase and end as white dwarfs (WDs), assuming a mean WD mass of $0.6M_\odot$. A fraction of these WDs will terminate their life as SNIa according to the next subsection. The ejected mass comprises processed elements (see section 2.7.6), while the energetics of AGBs winds is neglected.

2.7.5 Type Ia Supernovae

SNeIa are the final explosions of a C-O WD when it exceeds the Chandrasekhar mass ($1.44M_\odot$) by means of mass accretion from its companion in a binary system or through their merging. The SNIa rate depends on the mass ratio μ_i

of the primary or the secondary star with respect to the binary mass. Its distribution function and the probability of a star to be secondary in a binary system is described in Steyrleithner et al. (2020).

The number of SNIa N_{SNIa} in each mass bin can be calculated. The SNIa returns the complete final binary mass to the ISM with an energy efficiency of 5% of 10^{51} erg as for SNeII and a delay time after the star formation of about 60 Myr (Ploeckinger et al. 2014, see fig. 9) in agreement with Greggio (2010) and slightly shorter than values found by Maoz et al. (2012). Since SNeIa act as single explosion, we suggest that they stir-up the ISM more effectively than SNII explosions.

2.7.6 Chemical Feedback

At the end of its lifetime, a star not only returns mass in general to the ISM, but the material also comprises nucleosynthesis products, which lead to an enrichment of heavier elements as chemical feedback. SNeII enrich their surroundings mostly with α -elements like Ne and O, whereas SNeIa yield mostly Fe taken from the W7 model of Travaglio et al. (2004). For intermediate-mass stars their enrichment during the AGB phase is dominated by N and C. We use the stellar yields from Marigo et al. (1996) for stellar masses $m_* = (1-4)M_\odot$ and Portinari et al. (1998) for masses above $6M_\odot$ with a linear interpolation between 4 and $6M_\odot$.

3 RESULTS

3.1 The Evolution

Fig. 2 shows a snapshot at a simulation time of $t_{sim} = 1050$ Myr for both the filled and truncated IMF, respectively, as a density cut through the xz -plane at $y = 0$. The highest spatial resolution is in both cases 50 pc in each dimension. The truncated IMF (right panel) exhibits a strong galactic bipolar outflow, driven by the larger SFR and SNeII (see next sect. and sect. 3.3) rate. With velocities of up to 600 km s^{-1} a galactic wind is driven. The filled IMF on the left-hand side does not show such an outflow.

3.2 Star-Formation Rate

The SFR, is the most important process for the evolution of galaxies and is depicted in fig. 3 for both IMF modes, filled (solid line) and truncated (dashed line).

If the total SFR of a model exceeds the critical value of $10^{-2} M_\odot \text{ yr}^{-1}$ the formation of individual star clusters can fall beneath the critical mass for a full IMF (Ploeckinger et al. (2014)). In the case of the filled IMF, the actual presence of even numerical fractions in massive star bins allows the regulation of SF by feedback of all massive stars instantaneously. Importantly, the radiative energy release (Lyman continuum) depends on the stellar mass by a steeper positive power than the absolute value of the negative IMF slope (see eq. 16). This leads additionally to a somehow over-regulated SF with respect to the truncated IMF, resulting in a lower SFR as already seen in Ploeckinger et al. (2014).

Due to the lack of the most massive stars, the radiative stellar feedback of the truncated IMF is smaller and SNII

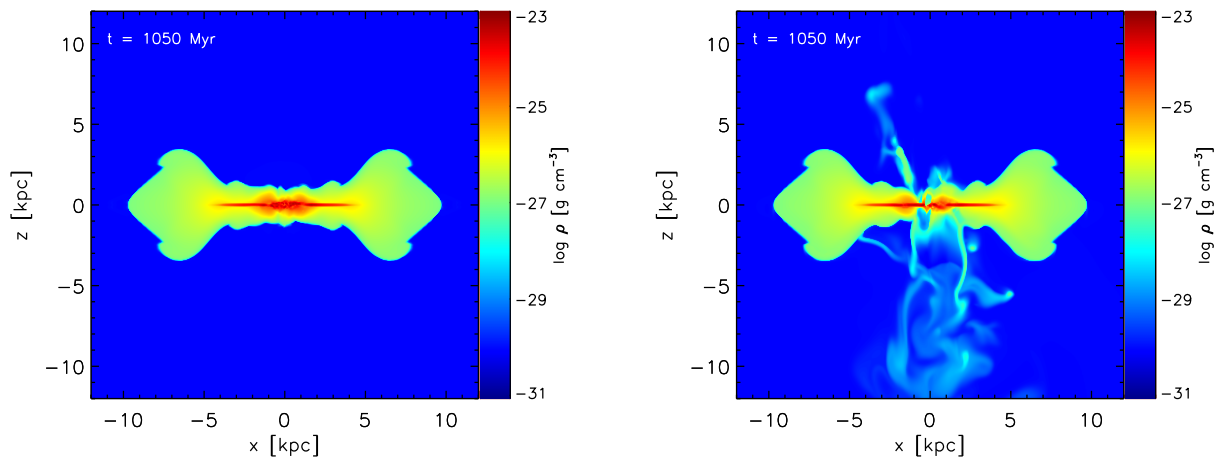


Figure 2. Edge-on slice through the filled IMF model (left) and truncated IMF model (right) at the same simulation time of $t_{sim} = 1050$ Myr. The truncated IMF exhibits a strong bipolar outflow due to a higher SFR and a locally weaker feedback compared to the filled IMF. The colour bar is given in logarithmic volume densities.

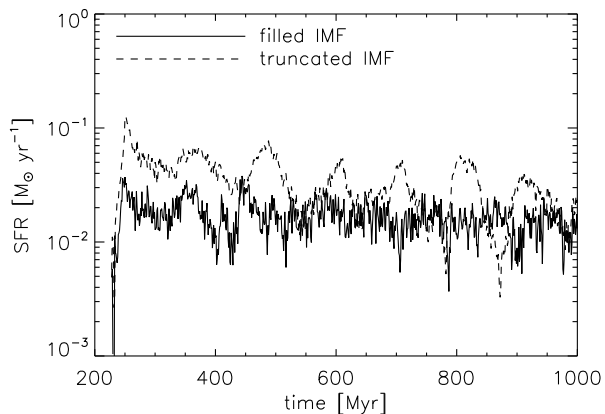


Figure 3. SFR in 1 Myr bins for the filled (solid line) and truncated (dashed line) IMF, respectively.

explosions are delayed due to the longer lifetime of the m_{max} stars and the lack of very short-lived stars. Both result in an initially larger SFR. The SF of the truncated IMF is further characterized by oscillations (see fig. 3) with periods around 120 Myr, almost the free-fall time of the DG. This so-called “breathing” happens here also for a flattened rotating disk DG, while Schroyen et al. (2011) discover its occurrence in non-rotating DG models.

3.3 Supernova type II Feedback

Fig. 4 shows the SNIi energies for both filled and truncated IMF, respectively, at the first 70 Myr of star formation. The solid and dashed lines indicate the average SNIi energy per Myr for the filled and truncated IMF, respectively. The dots (red for the filled and yellow for the truncated IMF) represent the SNIi energy of a single stellar cluster in the current

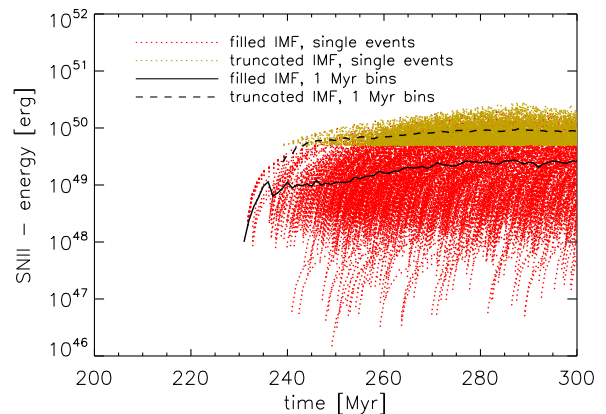


Figure 4. SNIi energy (5% of the total SNIi energy of 10^{51} erg) for the filled IMF (red dots and solid black line) and the truncated IMF (yellow dots and dashed black line). The lines are the SNIi energy in 1 Myr bins and the dots represent the SNIi energy for a single cluster at the current time step. Shown are the first 80 Myr of feedback from type II SNe.

timesteps. Chained dots towards the upper-right direction, most clearly discernible for the filled IMF (red), belong to the same star cluster and reveal the increasing SNIi number with the aging of the SSP. That many cluster SNeII start mostly below 10^{47} erg demonstrates that from massive stars only small fractions of SNIi energy is released. The lower cut-off at 5×10^{49} erg for the truncated IMF reflects directly the SNIi energy transfer efficiency of 5%.

This leads to lower temperatures of the hot expelled gas of about 10^5 K that cools more efficiently, which means that the thermal feedback by SNeII is reduced, even with the cooling procedure mentioned above. The thermal energy is

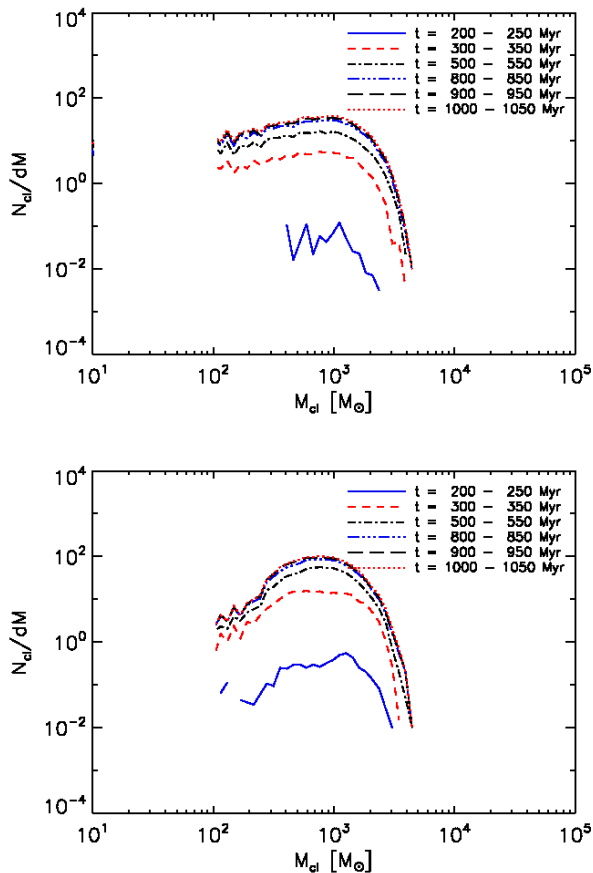


Figure 5. The cluster mass function in 50 Myr age bins for the filled IMF (top panel) and the truncated IMF (bottom panel) shows the number of clusters per initial mass bin (dM) as a function of the cluster mass.

thus too low and is efficiently cooled away to drive a galactic wind.

In contrast, the truncated model allows only explosions for integer SNII numbers in each mass bin, i.e. with more energetic SN power for each individual explosion. This can explain why a massive galactic wind is driven (right-hand fig. 2). At this stage it cannot be definitively concluded from the models which of both factors contributes more to the galactic wind, the stronger SFR or the larger SNII energy, or both. We will focus on this question analytically in sect. 4.2.

As one can also discern from fig. 4, the SNII feedback starts earlier for the filled IMF, because though only fractions, the lifetimes of the most massive stars are shortest. They explode already after a few Myr, while for the truncated IMF the SNeII are delayed.

3.4 Cluster Mass Function

Although the global SFR stays mostly above $10^{-2}M_{\odot}\text{yr}^{-1}$, i.e. filling the IMF in the case of a single star cluster, the cluster mass function (CMF) in fig. 5 shows cluster masses always below 10^4M_{\odot} , which is insufficient to complete the IMF.

For the CMF for the filled and truncated IMF, respec-

tively, one can notice, that the truncated IMF has more massive clusters than the filled IMF. The differences between the CMFs already start quite early, during the first 30 Myr of SF. The reasons for these are manifold: As already mentioned, the SF of the filled IMF gets more strongly regulated by the feedback of massive stars and with a larger power of released energy (see sec. 2.7.1) even for fractions of massive stars. Clusters with the truncated IMF have more time to accumulate mass within one Myr of cluster-formation time until they are capable of producing entire massive stars, which then start to regulate the SF by their feedback. Therefore, the truncated IMF initially forms more star clusters, resulting in a higher SFR at the beginning. After a simulation time of 250 Myr the difference in the CMF gets more pronounced, and the truncated IMF produces more massive clusters. Surprisingly, both peak at a cluster mass of $M_{cl} = 10^3M_{\odot}$. The difference is not that large for both CMFs in the amplitude of the peak, but in their shape.

That the CMF deviates from the global shape, must be interpreted as follows: With respect to the standard CMF slope $\frac{dN}{dM_{ecl}} \propto M_{ecl}^{\beta}$ of $\beta = -2$, at lower cluster masses the CMF flattens or even decreases (de Grijs et al. 2005; Larsen 2009) but in the massive range of $> 10^4M_{\odot}$, steepens to -2.7 and higher, e.g. Webb & Sills (2021, for M83). The compilation of CMFs from the recent literature by Krumholz et al. (2019), however, does not show a clear tendency of slopes from massive to less massive cluster ranges. This result supports any conclusion from the observations by Hunter et al. (2003) of $\beta \simeq -2.4$ for the Large and Small Magellanic Clouds (LMC and SMC) and de Grijs & Anders (2006) of $\beta = -1.8 \pm 0.1$ (LMC) and -2.00 ± 0.15 (SMC) that the CMF could be time-dependent. Moreover, the most important caveat for the comparison of our CMF with those literature values is that observed CMFs hardly reach below $M_{cl} \sim 10^4M_{\odot}$. Because of the low SFR in our simulations, clusters could also not gain such large masses as it was the case for TDGs where gas inflow enhances the star formation (Ploekinger et al. 2014). This supports the $M_{cl,max}$ -SFR correlation discussed before.

3.5 Chemical Abundances

In order to interpret deviations from a global IMF, abundance ratios of characteristic chemical elements are a crucial signature. Reasonably, the evolution of the chemical abundances between the filled and truncated IMF differ. Fig. 6 shows the time evolution of N, O, and Fe and their abundance ratios with an initial metallicity of $Z = 0.32Z_{\odot}$ as averaged values within a cylinder of $r = 0.5\text{kpc}$ and height $z = 0.2\text{kpc}$. The abundance ratio between two elements X_i is defined as

$$\left[\frac{X_1}{X_2} \right] = \log_{10} \left(\frac{X_1}{X_2} \right) - \log_{10} \left(\frac{X_1}{X_2} \right)_{\odot}. \quad (28)$$

There are some main properties when comparing the filled and the truncated IMF:

- (i) In the case of the filled IMF (fig. 6, top panel), the element abundances approach constant values, while those for the truncated IMF (bottom panel) increase.
- (ii) The [O/Fe] value of the ISM follows the typical SNII yields of ~ 0.3 , because at these short timescale the SNIa enrichment is delayed and still minor.

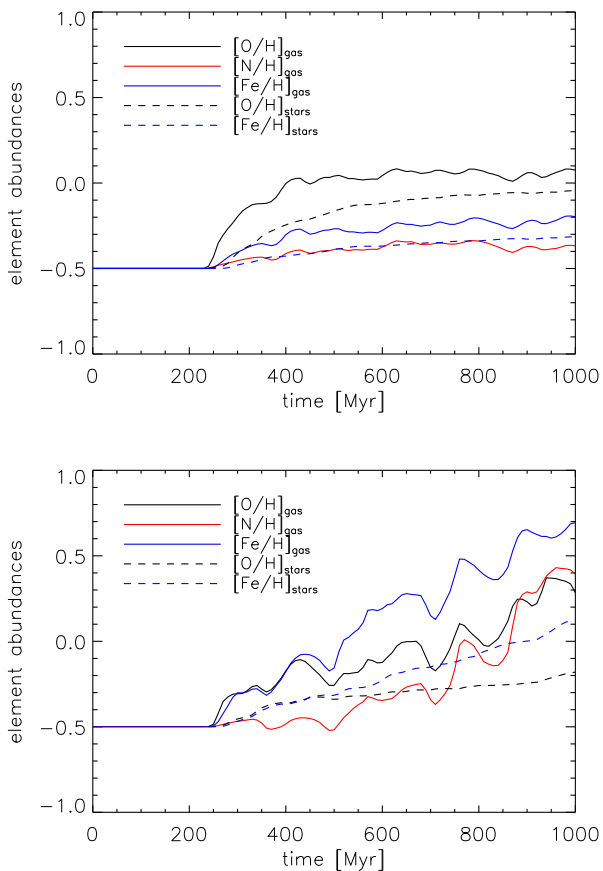


Figure 6. Element abundances for the gaseous (solid lines) and the stellar component (dashed lines) within the central region as a function of time. Top panel: filled IMF, bottom panel: truncated IMF.

(iii) The O and Fe abundance experience an unusual step rise after the first stellar generation injects its stellar products. This can be understood by a rough estimate: Since the abundance determinations are for both, gas and stars, the volume under consideration is limited to the star-forming central region, a flat central puck of ~ 1 kpc radius and 100 pc height. With the density of 1 cm^{-3} almost a million M_{\odot} are contained in this puck. A SFR of $10^{-2} M_{\odot}\text{ yr}^{-1}$ over 10^7 yr, i.e. the lifetime of about a $20 M_{\odot}$ star, allows the use of up to 10% of the gas, while the most massive stars are already injecting their chemical products. The continuation of star formation must therefore be supported by gas instream with the same initial metallicity of $1/3 Z_{\odot}$, i.e. an initial O content of $10^6 M_{\odot} \times 3 \cdot 10^{-3}$ O mass fraction. For a full IMF with $10^5 M_{\odot}$, almost 1/10 of the total stellar mass is processed and returned over the stellar lifetime of $2 - 3 \cdot 10^7$ yr and of this, 10% is O-rich, which results in $10^3 M_{\odot}$ oxygen or an increase of $\log [O/H]$ to -0.35 . After 10^8 years, 1% of the stellar mass returned already amounts to $10^4 M_{\odot}$ of oxygen and leads to a further growth, but with dilution due to dynamical effects. The differences between the IMF models are directly discernible in fig. 7.

(iv) The truncated IMF model starts with the same O and Fe enrichment, but has a slightly earlier Fe contribution.

This can be understood from the mass truncation so that the larger O production normalized to the IMF mass from the more massive stars, does not contribute here as it does for the full IMF.

(v) Well understood for both models independently, N remains below Fe and follows its enhancement with the same curvature, but very intriguingly the ratio of $[N/O]$ differs clearly: it has almost constant values of about -0.5 , while the truncated model varies strongly between -0.3 to even positive ratios.

While DGs follow the extension of a regular mass-metallicity relation down to low masses (Kirby et al. 2013) but with increasing scatter, particular element abundances and abundance ratios in DGs show a large variety, as e.g. sub-solar $[\alpha/Fe]$ in dwarf spheroidals and ultra-diffuse galaxies.

The reason for this behaviour could be, that the truncated IMF has, by definition, on average more integer massive stars, producing more SNeII which inject, therefore, more oxygen into the ISM. The filled IMF has, as already mentioned, fractions of massive star, and therefore will also inject fractions of stellar element abundances into the IMF by SNeII. Fig. 7 shows a slice through of the xz -plane of the volume density, $[N/H]$, $[O/H]$ and $[Fe/H]$ of the filled and truncated IMF. One can clearly see that the truncated IMF produces large superbubbles, that break out of the plane and are filled with higher element abundances. These reach values up to 1.5 of solar (in the case for $[Fe/H]$).

4 DISCUSSION

4.1 Numerical Models

The comparison between DG simulations with filled vs. truncated IMF, demonstrates the importance of handling the IMF in numerical simulations reasonably with regard to the SFR and the resulting cluster masses. Even under the assumption of an empirical IMF slope, low SFRs must guarantee the completeness of the stellar mass distribution i.e. the existence of integer star numbers as, e.g., by truncating the IMF or by random sampling. Ploekinger et al. (2014) and Elmegreen (2009) have independently demonstrated that a minimum cluster mass of about $10^4 M_{\odot}$ is required to fill the IMF according to the "universal" law, whereas below (e.g. $10^3 M_{\odot}$) it leads to a lack of the most massive stars and, by this, a deviation in the slope of the massive IMF range. Its relevance is caused by mainly two reasons: (i) While for a filled IMF the energy release by massive-star radiation sets in immediately and to a stronger power by even fractions of the most massive stars, in the truncated-IMF case the radiative feedback stems from the lower stellar mass in the massive range. By this, the SF self-regulation is stronger in the filled mode. (ii) With a filled IMF one can get fractions of massive stars which lead to a lower average SNII energy (see fig.4) injected into the ISM, whereas with a truncated IMF one ensures that only integer numbers of stars exist, with a higher mean mass. Even if the IMF of a star cluster is filled, its accumulated power of SNII explosions can drop beneath that of full stars in the truncated mode because their start is delayed and their full energy is released on a shorter timescale.

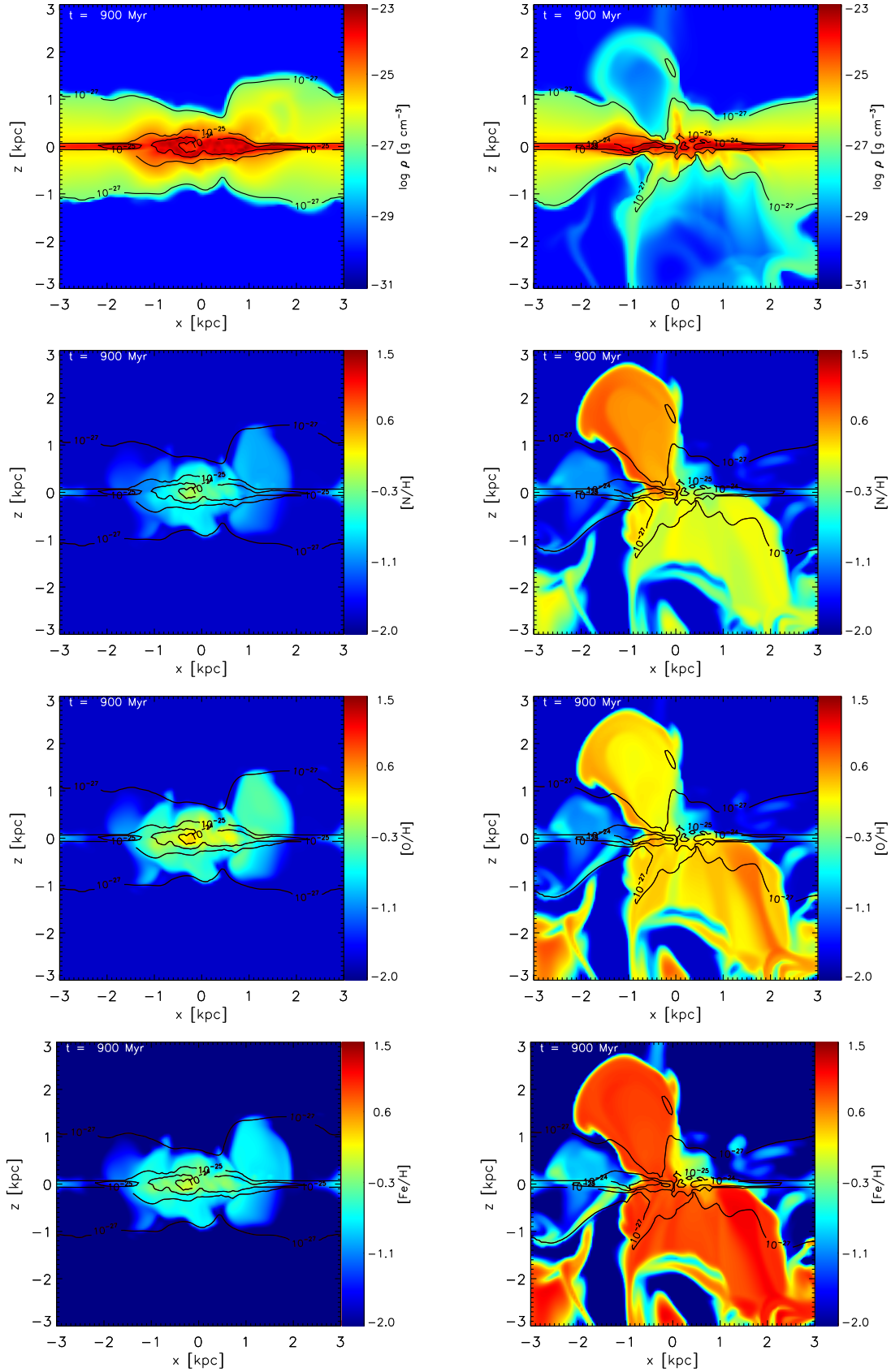


Figure 7. Slices through the xz -plane at $y=0$ at a simulation time of $t=900\text{ Myr}$ for the filled (left) and truncated (right) IMF, respectively. From top to bottom: density in $\log[\text{g cm}^{-3}]$, $[\text{N}/\text{H}]$, $[\text{O}/\text{H}]$ and $[\text{Fe}/\text{H}]$. Overlaid are density contours for 10^{-27} , 10^{-25} , $10^{-24} \text{ g cm}^{-3}$

This result of our simulations has to be considered with serious care because the SFRs are affected by the different IMF recipes in the sense that the lower in-situ self-regulation in the truncated IMF case inherently experiences a larger SFR. This effect can also be illustrated by fig. 5 where a truncated IMF produces more massive star clusters than a filled IMF.

Due to the formation of more massive stars in our model, this truncated IMF therefore also produces a larger SNII feedback, as discussed above, which drives a galactic wind. A normalization to equal SFRs allows a serious comparison of the IMF effects on the energetic feedback and will be presented in the next section.

The neglect of this energetic effect on the SF self-regulation could lead to major artefacts in numerical simulations of DGs when a filled IMF at low SFRs and too small cluster masses produces an unrealistic energy feedback. Since this IMF problem is irrelevant in many numerical simulations of massive galaxies, when high SFRs also lead to massive star clusters, this effect does not exist in low-mass DG models. Here the per mill fractions of SNII energy have the same effect as the well-known overcooling problem, because a temperature much lower than hot SN gas at about $10^4 - 10^5$ K can efficiently be cooled off. Mostly, the lack of sufficient SNII energy, e.g. in cases where modelers wish to drive a galactic wind artificially so as to solve the cusp-core problem in DGs according to the observed cored DM distribution (Governato et al. 2012), is commonly compensated by unrealistically high SN efficiencies (sometimes up to 100%) or an inconsistently high SFR. Agertz et al. (2011) state that in their simulations a total SNII feedback (with no SN efficiency) of 100%, even up to 500%, leads to a more realistic bulge-to-disc ratio.

The herewith questioned full-IMF recipe explains the divergence of Ha vs. UV brightnesses at SFRs below $10^{-2} M_{\odot} \text{yr}^{-1}$, e.g. Lee et al. (2009). If one considers that the SFR of DGs can reach even the order of $10^{-4} - 10^{-2} M_{\odot} \text{yr}^{-1}$, which leads to cluster masses that probably will not fill the IMF, the pure scope of DGs survival and their M/L ratio will also be affected. A truncated IMF provides both, a more realistic description of the IMF depending on the cluster mass and SFR, as well as a SN energy transfer efficiency, mostly between 5 – 15% as derived from single SN explosion models (Thornton et al. 1998), and not additionally reduced by a shortage of SN energy due to fractions.

The application of a truncated IMF will be quite useful when simulating e.g. ram-pressure stripped (RPS) DGs, firstly because of their low masses and low SFRs and secondly, when investigating star-forming RPS gas. Hester et al. (2010); Fumagalli et al. (2011); Yagi et al. (2013); Jáchym et al. (2014); Kenney et al. (2014); Johnson et al. (2015) derive active or recent SF in such gas tails with rates between $10^{-4} - 10^{-2} M_{\odot} \text{yr}^{-1}$. Moreover, the frequently doubted survival of DGs formed in the tidal tails of interacting systems which also show very low SFRs (e.g. Väisänen et al. (2008)) must be newly considered under this aspect (Ploekinger et al. 2014). And finally, the extrapolation of the past SFR history in early-type DGs and the derivation of energies and chemical abundances, requiring e.g. strong galactic winds in order to reduce the effective yield, must be reconsidered. As demonstrated, the chemical abundances are also affected by the implication of a truncated IMF. Instead of artificial

assumptions such as e.g. differential winds (Recchi et al. 2008) to understand low α -element abundances in low-mass galaxies, variations of the IMF should be taken into considerations.

4.2 An Analytic Comparison between filled vs. truncated IMF

Based on the two-fold IMF (eqs. 9 and 10), we wish here to obtain a general insight as to how truncated vs. filled IMF of a specified cluster mass, i.e. the upper-mass truncation, changes the energetic feedback. This was not yet possible from the numerical simulations above, because the self-consistent inherently higher SFR of the truncated IMF recipe does not allow the disentanglement of whether the galactic wind is caused by its resulting larger SNeII rate or whether the SNII power is higher due to the later onset of SNeII.

We consider a star cluster as a single stellar population in the formal mass range of $0.1 - 100 M_{\odot}$ for simplicity. Since we are interested in the question of how massive stars affect the energetic regulation by ionizing radiation, stellar winds, and SNII explosions, only the mass range above $8 M_{\odot}$ needs to be specified. We, therefore, split the mass range accordingly:

$$N_{tot} = k_1 \int_{0.1 M_{\odot}}^{0.5 M_{\odot}} m^{-1.3} dm + k_2 \left(\int_{0.5 M_{\odot}}^{8 M_{\odot}} m^{-2.3} dm + \int_{8 M_{\odot}}^{m_{max}} m^{-2.3} dm \right) \quad (29)$$

$$M_{tot} = k_3 \int_{0.1 M_{\odot}}^{0.5 M_{\odot}} m^{-0.3} dm + k_4 \left(\int_{0.5 M_{\odot}}^{8 M_{\odot}} m^{-1.3} dm + \int_{8 M_{\odot}}^{m_{max}} m^{-1.3} dm \right), \quad (30)$$

where only the right-hand terms will be evaluated.

For a "filled" IMF over the whole mass range up to $m_{max} = 100 M_{\odot}$ the stellar mass fraction contained in the lower mass range of $0.1 - 8 M_{\odot}$ (first two summands in eq. 30) amounts to 82.2%. For a minimally filled IMF, meaning that only a single $100 M_{\odot}$ star exists, and with 30 logarithmic mass bins dividing the mass range between 8 and $100 M_{\odot}$, the total cluster mass has to reach about $1.47 \times 10^4 M_{\odot}$. When we reduce this critical maximum mass m_{max} at which a single star is finally formed, lower cluster masses result (see tab. 1). We have to emphasize here already, that the results of this analytical study do not depend qualitatively on the number of mass bins as long as the massive-star range is properly sub-divided, i.e. the maximum bin is sufficiently wide enough to include the single stellar mass as demonstrated by Popescu & Hanson (2014). Quantitative uncertainties lie on the percentage level. For this simple analysis, we first truncate the IMF by fixing the maximum mass m_{max} at 100, 60, 40, 25, and 15 M_{\odot} arbitrarily and populate the uppermost mass bin with a single star, so that no star and even no fraction exist above m_{max} . For this truncated IMF, we calculate the total cluster masses. In the case of the "filled" IMF this mass is distributed accordingly over the whole mass range of $0.1 - 100 M_{\odot}$, leading to less mass per bin than in the truncated case. Consequently, in the filled IMF even the m_{max} bin and bins above are populated by number fractions of stars only, which also determine the stellar

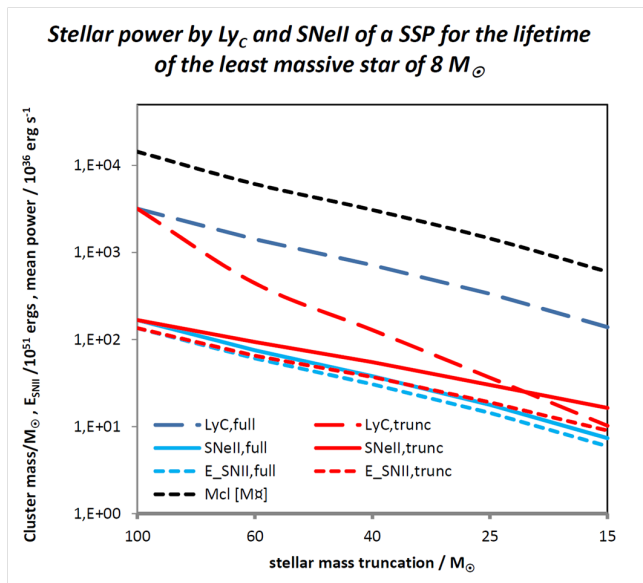


Figure 8. Cluster masses (black short-dashed line), Lyman continuum-radiation power (red/blue long-dashed lines) averaged over the maximum lifetime (of a $8M_{\odot}$ star), and supernovae type II power (red/blue full-drawn lines, with stellar lifetime delay), and total SNeII energies (red/blue short-dashed lines) over the most massive stellar mass m_{max} (values are listed in tab. 1). The power values are normalized to 10^{36}ergs^{-1} , the total SNeII energy release E_{SNeII} to 10^{51}erg , by this, directly counting the number of SNeII.

energy feedback. In fig. 8 the slope of the $m_{max} - \log(M_{cl})$ relation of the truncation amounts to $+0.0162$.

The presented models imply two sources of stellar energy feedback by massive stars: ionizing radiation and SNeII explosions, respectively. By the dependence of their power on stellar mass and numbers, differences in the energy release and their effects on the SF self-regulation can be expected and will be explored analytically here.

Concerning the Lyman continuum radiation, the Ly_c photon flux is a power-law function of the stellar mass $S_{Ly_c}(m) \propto m^{\beta}$ with a large exponent β of $+4$ as in eq. 16 or higher (e.g. $+6$ as derived by Hensler (1987)). Folding this $S_{Ly_c}(m)$ mass dependence with the IMF $\xi(m)$ power-law and the (mass-dependent) stellar lifetime with a power of almost -1.85 , the integration yields the total released Ly_c energy

$$E_{Ly_c} \propto \int_8^{m_{max}} S_* \xi(m) \tau_*(m) dm \propto \int_8^{m_{max}} m^{0.85} dm \propto m_{max}^{1.85} - 46.85, \quad (31)$$

leading to a positive power with the maximum mass. This also means that the “filled” IMF, even with mass fractions in the massive-stars’ mass bins - in reality impossible, but numerically treatable - produces more Ly_c energy than a truncated one and thus exerts a stronger radiative feedback (see fig. 8).

The Ly_c radiation acts with a larger power for the filled IMF because the most massive stars exist even with fractions. For the lowest considered truncated cluster mass of $15M_{\odot}$, this difference amounts to a factor of 13 (tab. 1).

This situation changes when we consider the SNeII energy of both IMF modes. Although the total masses of massive stars only differs insignificantly, i.e. by less than 1%, between the full and the truncated IMF (tab. 1), the mass in the occupied bins is up to a factor of 2.4 larger in the truncated IMF. This also holds for the numbers of stars. As a side note, it should be mentioned that the star numbers of the truncated IMF are reasonably all set to integer values, while those of the filled IMF have floating values.

The stellar radiative energy feedback by Ly_c photons acts almost continuously during the stellar lifetime, while SNeII explosions are instantaneous events for each star, terminating its life. However, for an ensemble of stars with multiple SNeII from the energetic point of view, these events, for simplicity, can be smeared out and treated as a continuous energy source. This means, that the sum of SN explosions is taken into account for a time interval from the first occurrence by the shortest-living most massive progenitor star m_{max} until the deaths of the least massive exploding stars, i.e. at $8M_{\odot}$. Although the total energy of SNeII (see tab. 1) deviates at most for the $m_{max} = 15M_{\odot}$ model by a factor of 1.5, their ratio in the SNeII power E_{SNeII} grows to 2.2, caused by the shrinkage of the considered time interval from the m_{max} stars to $8M_{\odot}$.

As one recognizes from fig. 8, the M_{cl} curve declines parallelly to the power of SNeII in the full-IMF mode. The ratio of L_{SNeII}/M_{cl} amounts to $3.22L_{\odot}M_{\odot}^{-1}$.

5 CONCLUSIONS

In the presented study, we aim at demonstrating by numerical and analytical models, which consequences the neglect of a possible non-standard IMF bear for numerical simulations in cases of low SFRs. We apply the simplified approach to fill the IMF from low stellar masses up to a maximum mass at which a full star can be formed. This treatment leads to different star cluster IMFs: truncated IMF when the gas reservoir is consumed and full stellar IMF population otherwise. This model with IMF truncation is compared with numerical evolution models of DGs where the IMF is always completely filled even when the IMF allows only fractions of massive stars to be formed. The energetic difference of a filled cluster IMF, despite the concession of star fractions, vs. the truncated IMF, the latter based on complete stars only, are elaborated and strikingly shown: a filled IMF, even by fractions of massive stars, regulates the SF more intensively due to the steep $Ly_c(m)$ power-law than a truncated (or stochastic) IMF. This effect can be called SF over-regulations because of the exaggerated energy release. In contrast, the mass fractions of massive stars also contribute only fractions of full SN energy and, by this, does not energize the ISM sufficiently so that cooling at lower temperatures emits the energy too efficiently. It is therefore not sufficient to include SNeII as the only stellar feedback process, because as emphasized the SF self-regulation depends inherently on the Ly_c energetics.

The main take-away messages from our models are: At first, although low SFRs e.g. in DGs can produce star clusters which are completely filled by integer stars up to the uppermost mass limit of the IMF, individual

Table 1. Comparison of the cluster mass M_{cl} , to form the most massive star with mass m_{max} , the SFR to form this cluster mass, the Lyman continuum energy $E_{Ly\alpha}$, the number of type II SNe N_{SNeII} , and the feedback power $L_{Ly\alpha}$ and L_{SNeII} by Lyman continuum radiation and SNeII, respectively, for filled (full) and truncated (trunc.) IMF. For definition of IMFs see sec. 2.6.

		$m_{max} [M_{\odot}]$	100	60	40	25	15
$M_{cl} [M_{\odot}]$			14388	6120	3082	1448	599
SFR [$M_{\odot} \text{yr}^{-1}$]			1.49×10^{-2}	6.12×10^{-3}	3.08×10^{-3}	1.45×10^{-3}	5.99×10^{-4}
total mass [M_{\odot}]	full		2619	1087	547.5	257.3	106.4
$E_{Ly\alpha} [10^{51} \text{erg}]$	full		2570	1170	589	277	114
	trunc.		2570	357	104	29.4	8.23
$L_{Ly\alpha} [10^{37} \text{ergs}^{-1}]$	full		318	143	71.5	33.6	13.9
	trunc.		318	44.3	12.8	3.65	1.02
N_{SNeII}	full		135.0	62.0	31.2	14.7	6.07
	trunc.		135	65	37	19	9
$L_{SNeII} [10^{37} \text{ergs}^{-1}]$	full		16.7	7.53	3.79	1.78	0.737
	trunc.		16.7	9.37	5.49	3.00	1.64

star clusters exist which lack a completely filled IMF. Secondly, comparing the two extreme cases of filled vs. truncated IMFs leads to the mentioned energetic differences in star-formation self-regulation and SNII energy release. And thirdly, the reduced number of massive stars by a non-standard IMF leaves chemical signatures of enhanced abundance ratios of elements from intermediate-mass to massive stellar progenitors. This latter question and the derivation of SFRs from $H\alpha$ luminosities will be addressed in a forthcoming paper. In order to get a deeper insight into the issues of truncated vs. filled IMF approaches, we consider both for single stellar clusters of various masses analytically. The results demonstrate the above-mentioned deviations and agree well with the $M_{cl} - m_{max}$ relations depicted by Weidner et al. (2010). We also test the mass distribution in single star clusters by random sampling in order to compare it with the truncation approach. We can show that the median of 100 sampling runs for each cluster mass yields an uppermost mass at almost the same range (Hein, BSc thesis, Univ. of Vienna) as the truncation method. From this, one can also conclude that for a given star cluster mass the truncation provides a more easily manageable method than a random sampling procedure.

DATA AVAILABILITY

The data underlying this article will be shared on reasonable request to the corresponding author. The used and described code is available at the Flash Center at the University of Chicago and our extensions are described in section 2.

ACKNOWLEDGEMENTS

The authors benefit from multiple discussions with Pavel Kroupa, Sylvia Ploekinger, and Simone Recchi, as well as with Janice Lee, Bruce Elmegreen, and Takuji Tsujimoto. The authors acknowledge the proof reading by Shelley-Anne Deborah Harrisberg. We also acknowledge the positive report by an anonymous referee and supportive com-

ments which helped to improve the clarity of the paper. The software used in this work was in part developed by the DOE NNSA-ASC OASCR Flash Center at the University of Chicago. The computational results presented here have been achieved using the Vienna Scientific Cluster (VSC) under project no. 70670.

REFERENCES

- Agertz O., Teyssier R., Moore B., 2011, *MNRAS*, **410**, 1391
André P., Arzoumanian, D. Könyves, V. Shimajiri, Y. Palmeirim, P. 2019, *A&A*, **629**, L4
Andrews J. E., et al., 2013, *ApJ*, **767**, 51
Andrews J. E., et al., 2014, *ApJ*, **793**, 4
Applebaum E., Brooks A. M., Quinn T. R., Christensen C. R., 2020, *MNRAS*, **492**, 8
Baugh C. M., Lacey C. G., Frenk C. S., Granato G. L., Silva L., Bressan A., Benson A. J., Cole S., 2005, *MNRAS*, **356**, 1191
Baumschlager B., Hensler G., Steyrleithner P., Recchi S., 2018, *Monthly Notices of the Royal Astronomical Society*, **483**, 5315
Bekki K., 2013, *MNRAS*, **436**, 2254
Boehringer H., Hensler G., 1989, *A&A*, **215**, 147
Bonnell I. A., Bate M. R., Vine S. G., 2003, *MNRAS*, **343**, 413
Boselli A., Boissier S., Cortese L., Buat V., Hughes T. M., Gavazzi G., 2009, *ApJ*, **706**, 1527
Boselli A., et al., 2018, *A&A*, **615**, A114
Calzetti D., Chandar R., Lee J. C., Elmegreen B. G., Kennicutt R. C., Whitmore B., 2010, *ApJ*, **719**, L158
Chabrier G., 2003, *PASP*, **115**, 763
Chamandy L., Shukurov A., 2020, *Galaxies*, **8**, 56
Conroy C., van Dokkum P., 2012, *ApJ*, **747**, 69
Dalgarno A., McCray R. A., 1972, *ARA&A*, **10**, 375
Dib S., Schmeja S., Hony S., 2017, *MNRAS*, **464**, 1738
Eldridge J. J., 2012, *MNRAS*, **422**, 794
Elmegreen B. G., 2000, *ApJ*, **539**, 342
Elmegreen B. G., 2006, *The Astrophysical Journal*, **648**, 572
Elmegreen B. G., 2009, in Sheth K., Noriega-Crespo A., Ingalls J. G., Paladini R., eds, *The Evolving ISM in the Milky Way and Nearby Galaxies*. p. 14 ([arXiv:0803.3154](https://arxiv.org/abs/0803.3154))
Elmegreen D. M., et al., 2014, *The Astrophysical Journal*, **787**, L15
Faesi C. M., Lada C. J., Forbrich J., 2019, *VizieR Online Data Catalog*, p. [J/ApJ/857/19](https://arxiv.org/abs/1907.08571)

- Ferreras I., La Barbera F., de La Rosa I. G., Vazdekis A., de Carvalho R. R., Falcon-Barroso J., Ricciardelli E., 2013, *MNRAS*, **429**, L15
- Freyer T., Hensler G., Yorke H. W., 2003, *ApJ*, **594**, 888
- Freyer T., Hensler G., Yorke H. W., 2006, *ApJ*, **638**, 262
- Fryxell B., et al., 2000, *ApJS*, **131**, 273
- Fumagalli M., Gavazzi G., Scaramella R., Franzetti P., 2011, *AA*, **528**, A46
- Gatto A., et al., 2017, *MNRAS*, **466**, 1903
- Governato F., et al., 2012, *MNRAS*, **422**, 1231
- Grasha K., et al., 2019, *MNRAS*, **483**, 4707
- Greggio L., 2010, *MNRAS*, **406**, 22
- Hensler G., 1987, *Mitteilungen der Astronomischen Gesellschaft Hamburg*, **70**, 141
- Hensler G., 2007, in Emsellem E., Wozniak H., Massacrier G., Gonzalez J. F., Devriendt J., Champavert N., eds, *EAS Publications Series Vol. 24*, *EAS Publications Series*. pp 113–118 ([arXiv:0709.0631](https://arxiv.org/abs/0709.0631)), doi:10.1051/eas:2007018
- Hensler G., Theis C., Gallagher III. J. S., 2004, *A&A*, **426**, 25
- Hester J. A., et al., 2010, *ApJL*, **716**, L14
- Hunter D. A., Elmegreen B. G., Dupuy T. J., Mortonson M., 2003, *AJ*, **126**, 1836
- Jáchym P., Combes F., Cortese L., Sun M., Kenney J. D. P., 2014, *ApJ*, **792**, 11
- Jeffreson S. M. R., Krumholz M. R., Fujimoto Y., Armillotta L., Keller B. W., Chevance M., Kruijssen J. M. D., 2021, *MNRAS*, **505**, 3470
- Johnson M. C., et al., 2015, *MNRAS*, **451**, 3192
- Johnson L. C., et al., 2017, *ApJ*, **839**, 78
- Kenney J. D. P., Geha M., Jáchym P., Crowl H. H., Dague W., Chung A., van Gorkom J., Vollmer B., 2014, *ApJ*, **780**, 119
- Kennicutt Robert C. J., 1998, *ApJ*, **498**, 541
- Kirby E. N., Cohen J. G., Guhathakurta P., Cheng L., Bullock J. S., Gallazzi A., 2013, *ApJ*, **779**, 102
- Koeppen J., Theis C., Hensler G., 1995, *A&A*, **296**, 99
- Kroupa P., 2001, *MNRAS*, **322**, 231
- Kroupa P., 2002, *Science*, **295**, 82
- Kroupa P., 2014, *Astrophysics and Space Science Proceedings*, **36**, 335
- Kroupa P., Weidner C., Pflamm-Altenburg J., Thies I., Dabringhausen J., Marks M., Maschberger T., 2013, *The Stellar and Sub-Stellar Initial Mass Function of Simple and Composite Populations*. p. 115, doi:10.1007/978-94-007-5612-0_4
- Krumholz M. R., 2014, *Phys. Rep.*, **539**, 49
- Krumholz M. R., McKee C. F., Bland-Hawthorn J., 2019, *ARA&A*, **57**, 227
- Kudritzki R. P., Pauldrach A., Puls J., 1987, *A&A*, **173**, 293
- Lada C. J., Lada E. A., 2003, *ARA&A*, **41**, 57
- Larsen S. S., 2002, *AJ*, **124**, 1393
- Larsen S. S., 2009, *A&A*, **494**, 539
- Larson R. B., 1988, in Pudritz R. E., Fich M., eds, *NATO Advanced Study Institute (ASI) Series C Vol. 232*, *Galactic and Extragalactic Star Formation*. p. 459, doi:10.1007/978-94-009-2973-9_27
- Lee-Waddell K., et al., 2016, *MNRAS*, **460**, 2945
- Lee-Waddell K., Madrid J. P., Spekkens K., Donzelli C. J., Koribalski B. S., Serra P., Cannon J., 2018, *MNRAS*, **480**, 2719
- Lee H.-c., Gibson B. K., Flynn C., Kawata D., Beasley M. A., 2004, *MNRAS*, **353**, 113
- Lee J. C., et al., 2009, *ApJ*, **706**, 599
- Lombardi M., Alves J., Lada C. J., 2015, *A&A*, **576**, L1
- Loubser S. I., Hoekstra H., Babul A., Bahé Y. M., Donahue M., 2020, *Monthly Notices of the Royal Astronomical Society*, **500**, 4153
- Maeder A., 1996, in Leitherer C., Fritze-von-Alvensleben U., Huchra J., eds, *Astronomical Society of the Pacific Conference Series Vol. 98*, *From Stars to Galaxies: the Impact of Stellar Physics on Galaxy Evolution*. p. 141
- Maoz D., Mannucci F., Brandt T. D., 2012, *MNRAS*, **426**, 3282
- Marigo P., Bressan A., Chiosi C., 1996, *A&A*, **313**, 545
- Martín-Navarro I., et al., 2015, *ApJ*, **806**, L31
- McWilliam A., Wallerstein G., Mottini M., 2013, *The Astrophysical Journal*, **778**, 149
- Melekh B., Recchi S., Hensler G., Buhajenko O., 2015, *MNRAS*, **450**, 111
- Meurer G. R., et al., 2009, *ApJ*, **695**, 765
- Nagashima M., Lacey C. G., Okamoto T., Baugh C. M., Frenk C. S., Cole S., 2005, *MNRAS*, **363**, L31
- Pelkonen V.-M., Padoan P., Haugbølle T., Nordlund Å., 2021, *Monthly Notices of the Royal Astronomical Society*, **504**, 1219
- Pflamm-Altenburg J., Weidner C., Kroupa P., 2007, *ApJ*, **671**, 1550
- Ploekinger S., Hensler G., Recchi S., Mitchell N., Kroupa P., 2014, *MNRAS*, **437**, 3980
- Ploekinger S., Recchi S., Hensler G., Kroupa P., 2015, *MNRAS*, **447**, 2512
- Popescu B., Hanson M. M., 2014, *ApJ*, **780**, 27
- Portinari L., Chiosi C., Bressan A., 1998, *A&A*, **334**, 505
- Recchi S., Hensler G., 2013, *A&A*, **551**, A41
- Recchi S., Spitoni E., Matteucci F., Lanfranchi G. A., 2008, *A&A*, **489**, 555
- Recchi S., Calura F., Kroupa P., 2009, *A&A*, **499**, 711
- Roychowdhury S., Chengalur J. N., Begum A., Karachentsev I. D., 2009, *MNRAS*, **397**, 1435
- Salpeter E. E., 1955, *ApJ*, **121**, 161
- Schroyen J., de Rijcke S., Valcke S., Cloet-Osselaer A., Dejonghe H., 2011, *MNRAS*, **416**, 601
- Schure K. M., Kosenko D., Kaastra J. S., Keppens R., Vink J., 2009, *A&A*, **508**, 751
- Smith R. J., 2020, *ARA&A*, **58**, 577
- Smith M. C., 2021, *MNRAS*, **502**, 5417
- Steyrleithner P., Hensler G., Boselli A., 2020, *Monthly Notices of the Royal Astronomical Society*, **494**, 1114
- Taylor E. N., et al., 2011, *MNRAS*, **418**, 1587
- Theis C., Burkert A., Hensler G., 1992, *A&A*, **265**, 465
- Thornton K., Gaudlitz M., Janka H. T., Steinmetz M., 1998, *ApJ*, **500**, 95
- Travaglio C., Hillebrandt W., Reinecke M., Thielemann F. K., 2004, *A&A*, **425**, 1029
- Tsujimoto T., 2011, *The Astrophysical Journal*, **736**, 113
- Tsujimoto T., Bekki K., 2011, *A&A*, **530**, A78
- Väisänen P., et al., 2008, *MNRAS*, **384**, 886
- Valcke S., de Rijcke S., Dejonghe H., 2008, *MNRAS*, **389**, 1111
- Vorobyov E. I., Recchi S., Hensler G., 2012, *A&A*, **543**, A129
- Vorobyov E. I., Recchi S., Hensler G., 2015, *A&A*, **579**, A9
- Webb J. J., Sills A., 2021, *MNRAS*, **501**, 1933
- Weidner C., Kroupa P., 2005, *ApJ*, **625**, 754
- Weidner C., Kroupa P., 2006, *MNRAS*, **365**, 1333
- Weidner C., Kroupa P., Bonnell I. A. D., 2010, *MNRAS*, **401**, 275
- Weidner C., Kroupa P., Pflamm-Altenburg J., Vazdekis A., 2013, *MNRAS*, **436**, 3309
- Weisz D. R., et al., 2012, *ApJ*, **744**, 44
- Weisz D. R., et al., 2015, *ApJ*, **806**, 198
- Yagi M., Gu L., Fujita Y., Nakazawa K., Akahori T., Hattori T., Yoshida M., Makishima K., 2013, *ApJ*, **778**, 91
- de Grijs R., Anders P., 2006, *MNRAS*, **366**, 295
- de Grijs R., Parmentier G., Lamers H. J. G. L. M., 2005, *MNRAS*, **364**, 1054

This paper has been typeset from a $\text{\TeX}/\text{\LaTeX}$ file prepared by the author.